IEEE Access
Multidisciplinary | Rapid Review | Open Access Journal

Received March 4, 2018, accepted April 23, 2018, date of publication May 10, 2018, date of current version June 5, 2018.

Digital Object Identifier 10.1109/ACCESS.2018.2834144

Enhanced Efficiency BPSK Demodulator Based on One-Dimensional Convolutional Neural Network

MIN ZHANG[1], ZONGYAN LIU[2], LI LI[3,4], AND HAI WANG[1], (Member, IEEE)

[1]School of Aerospace Science and Technology, Xidian University, Xi'an 710071, China
[2]School of Mechano-Electronic Engineering, Xidian University, Xi'an 710071, China
[3]School of Aeronautics, Northwestern Polytechnical University, Xi'an 710129, China
[4]China Academy of Space Technology, Xi'an 710100, China

Corresponding author: Hai Wang (wanghai@mail.xidian.edu.cn)

This work was supported by the Fundamental Research Funds for the Central Universities of China under Grant JB160409.

ABSTRACT In this paper, a novel binary phase shift keying demodulator based on 1-D convolutional neural network (1-D CNN) is proposed. The utilization of neural networks to detect the locations of phase shifts in the modulated data distinguishes the proposed scheme from other neural network demodulators, which decide the symbols corresponding to the sampled data in a symbol period. Meanwhile, coordinating with the symbol synchronization algorithm, the proposed structure is able to deal with the carrier frequency offsets and sampling frequency errors. Compared to the conventional demodulators, the proposed 1-D CNN demodulator presents better bit error rates performance.

INDEX TERMS Artificial neural networks, demodulation, AWGN channels, phase shift keying.

I. INTRODUCTION

Binary phase shift keying (BPSK) is the simplest scheme of the phase shift keying (PSK), which utilizes the phase shifts of the modulated signals to transmit digital information [1]. It is relatively easy to implement, and presents optimal anti-noise capability among PSK schemes. As a result, the BPSK technique has been widely used in the fields of satellite communication, deep space communication, and biomedical implant transceivers [2]–[4]. For conventional demodulators, the demodulation performance relies on the parameters of each module such as filters and phase detectors [5], which is time-consuming and complicated in implementation.

Neural network is a nonlinear model, which solves the nonlinear classification problem through the combination and superposition of the multiple perceptrons [6], and it is suitable for various applications in the field of communication [7]–[13]. Compared with conventional demodulators, neural network demodulators do not require respective designs for the parameters of each module, and its demodulation function is achieved through learning a large amount of modulated data. Therefore, it provides better flexibility and self-adaptability. Furthermore, because the neural networks learn some of the noise patterns in training process, it has better anti-noise capability. In recent years, many researches are focusing on the applications of neural network in digital demodulation.

A neural network amplitude shift keying (ASK) demodulator is proposed in [14], which combines the wideband noise rejection, pulse waveform shaping and decoding into one neural network, and these functions can be self-organized through the learning process. In [15], a multiuser code division multiple access (CDMA) demodulator and equalizer is reported, which is constructed by the mixed structure of the radial basis function (RBF) neural network and multi-layer perceptron (MLP). This structure presents better performance for channels with harsh environments. Amini and Balarastaghi [16] exploit a time delay neural network (TDNN) to perform the binary frequency shift keying (BFSK) demodulation. In the paper, two neural network demodulators which are separately trained with noisy data and noiseless data are compared. It is concluded that the demodulator trained by noisy data provides a better performance. He *et al.* [17] present a universal demodulator to deal with multiple modulation schemes and different scenes of modulation, where multiple MLPs are utilized to construct a demodulator named Max-Multiple Layer Perceptron, and the performance of the demodulator in different phase deviation are compared. A three-layer MLP structure served as multiple phase shift keying (MPSK) demodulator is proposed in [18], simulation results in additive white Gaussian noise (AWGN) channels and multipath channels are presented to illustrate that the demodulator can estimate and eliminate the undesired effects in the channels. Besides, a Gaussian minimum shift-keying (GMSK) demodulator based on the laming vector quantization (LVQ) neural networks is reported in [19], and an Elman neural network demodulator for frequency shift

keying (FSK) demodulation is described in [20]. Recently, a deep belief network (DBN) based demodulator is proposed in [21]. A demodulator for frequency modulation (FM) is introduced in [22], which utilizes the prior information of transmitted speech message in the demodulation process.

For the neural network demodulators mentioned in [14]–[20], the principle of the neural network is to map the modulated data within one symbol period into one symbol. This requires grouping the sequence of samples according to the symbol period, and treats each group of samples as an input vector of the neural network. However, since the Starting point of the symbol period is hard to find, grouping the sampling points during the demodulation process is with great difficulty. Moreover, due to the Doppler frequency shifts and sampling time error, the sampling phase deviation will be introduced in grouping the samples. Additionally, when the phase deviation is too large, the input vector of the neural network could no longer represent one symbol period, and that results in incorrect result of the demodulation.

Due to the fact that the PSK modulation transforms digital information into phase changes, the transmitted data can be extracted from the locations of phase shifts. In this paper, a neural network demodulator based on one-dimensional convolutional neural network (1-D CNN) is proposed. In contrast to other reported neural network demodulators, the proposed structure puts forward a demodulation method that judges the occurrence of the phase shifts in the sampled data and reconstructs the transmitted data based on the locations of phase shifts, therefore the proposed 1-D CNN demodulator does not suffer from grouping the sampled data. Benefitting from the symbol synchronization module, the 1-D CNN demodulator is able to deal with the phase deviation and Doppler frequency offset. In addition, the 1-D CNN demodulator structure uses two convolutional neural networks (CNNs) to detect two different types of phase shifts separately, which simplifies the complexity of features that each neural network needs to detect, and such that the demodulator presents a stronger anti-noise capability.

The rest of this paper is organized as follows. Section II introduces the structure of the BPSK modulation and the principles of the conventional BPSK demodulators. Section III describes the architecture of the proposed 1-D CNN demodulator, including a detailed description of the training set generation as well as the design of 1-D CNN. An analysis to carrier frequency offset handling is also given in this section. In section IV, the simulation results are provided and analyzed. Finally, Section V summarizes this paper.

II. CONVENTIONAL BPSK DEMODULATOR

For the BPSK modulation process, assuming the modulated signal is $x_s(t)$, the modulated BPSK signal in time domain can be expressed as

$$x_s(t) = A\cos(\omega_c t + \varphi_n) \tag{1}$$

where A denotes the maximum amplitude of the modulated signal, ω_c is the angular frequency of the carrier, φ_n is the phase of the modulated signal and represents the absolute phase of the nth symbol, which take the value of either 0 or π. Hence, $x_s(t)$ can be expressed as

$$x_s(t) = \begin{cases} A\cos(\omega_c t), & \varphi_n = 0 \\ -A\cos(\omega_c t), & \varphi_n = \pi \end{cases} \tag{2}$$

These two phases represent the two symbols 0 and 1, respectively. The signals of two symbols have the same waveform but the opposite polarities. Hence, they can be generally expressed as the multiplication of a bipolar rectangular pulse sequence and a sinusoidal carrier

$$x_s(t) = s(t)\cos(\omega_c t) \tag{3}$$

in which

$$s(t) = \sum_n a_n g(t - nT_s) \tag{4}$$

where $g(t)$ stands for a single rectangle pulse with a pulse width of T_s, and a_n takes two values, 1 or -1. Assume the received signal which has been modulated is represented by $x_r(t)$, and $x_n(t)$ represents the white Gaussian noise. Hence, the received signal can be expressed as

$$x_r(t) = x_s(t) + x_n(t) \tag{5}$$

A typical BPSK modulation adopting the scheme of coherent demodulation is diagramed in Fig. 1. The received modulated signal, $x_r(t)$, passes through the band pass filter (BPF) to eliminate the out-of-band noise, providing $x_r'(t)$. $x_r'(t)$ is multiplied with the local carrier, which is a sinusoidal signal generated through the carrier synchronization process and is expressed as

$$c(t) = \cos(\omega_0 t + \Delta\varphi) \tag{6}$$

The outcome of the multiplication can be calculated by

$$\begin{aligned} x_c(t) &= x_r'(t)c(t) = [s(t)\cos(\omega_c t) + \eta]\cos(\omega_0 t + \Delta\varphi) \\ &= s(t)[\cos((\omega_c - \omega_0)t - \Delta\varphi) - \cos((\omega_c + \omega_0)t + \Delta\varphi)] \\ &\quad + \eta \end{aligned} \tag{7}$$

where $\Delta\varphi$ denotes the phase difference between the local carrier and the modulated signal. ω_0 and ω_c denote the angular frequency of local carrier and the modulated signal, and the interference signals are all represented by η. The output of the low pass filter (LPF), $x_f(t)$, can be represented as

$$x_f(t) = s(t)\cos((\omega_c - \omega_0)t - \Delta\varphi) + \eta \tag{8}$$

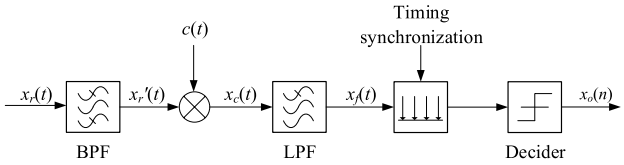

FIGURE 1. Procedures of coherent demodulation, where BPF is the abbreviation of band-pass filter, and LPF is the abbreviation of low-pass filter.

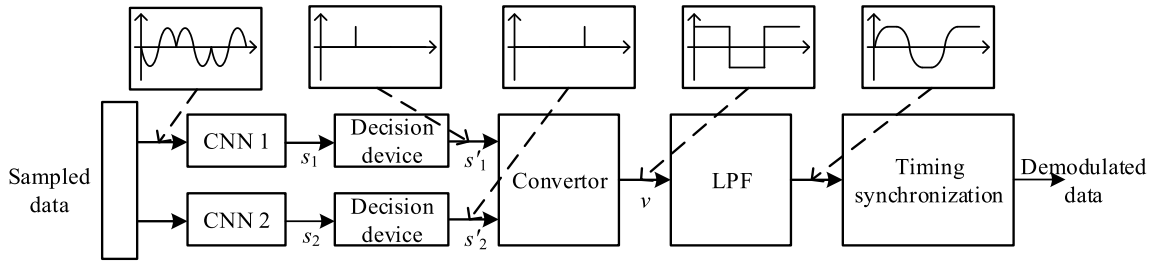

FIGURE 2. Structure of the proposed 1-D CNN demodulator and the output waveform of each module, including the sampled data, the outputs of decision device, the outputs of convertor, and the outputs of low-pass filter.

Then, $x_f(t)$ is transmitted to the symbol synchronization module, and the timing sampling is operated on $x_f(t)$. Finally, the transmitted data, $x_o(n)$, which represents the demodulation output is formed. As shown in (8), when the frequency and the phase of the local carrier are equal to those of the modulated signal, the transmitted data is accurately achieved from the modulated signal. Otherwise, the loss of the demodulation is produced.

III. PROPOSED 1-D CNN DEMODULATOR

Conventional BPSK coherent demodulators require carrier synchronization, which may lead to demodulation error when phase error and frequency offset exist during the synchronization. Fortunately, the proposed 1-D CNN demodulator directly loads the sampled data of the received modulated signals into the neural network, without carrier synchronization. The neural network accomplishes the demodulation by detecting the phase shift points of the modulated signals and extracting the phase information.

A. STRUCTURE OF THE PROPOSED DEMODULATOR

After the modulated signal is received, the analog to digital conversion (ADC) is employed first, and then the sampled data is demodulated by the proposed demodulator. The proposed 1-D CNN demodulator consists of two CNNs, two decision devices, a convertor, a LPF, and a symbol synchronization module. Fig. 2 shows the structure of the proposed 1-D CNN demodulator.

The information carried by PSK modulated signals is contained within the phase changes. For BPSK signals, only two phases are contained. Hence, the BPSK demodulator only needs to detect two kinds of phase shifts. In this paper, the proposed 1-D CNN demodulator is composed of two 1-D CNNs, where CNN 1 detects the phase shifts from 0° to 180°, and CNN 2 detects the phase shifts from 180° to 0°. If the neural network outputs 1, it represents that the specified feature of phase shift occurs in the input vector, and the output of 0 indicates that no specified feature of phase shift occurs. After the 1-D CNN going through all the consecutive samples, a series of outputs are obtained. Sequences s_1 and s_2 are achieved by permuting these outputs in a chronological order.

Fig. 3 shows the corresponding waveforms of the inputs with respect to the expected outputs. Since the outputs of

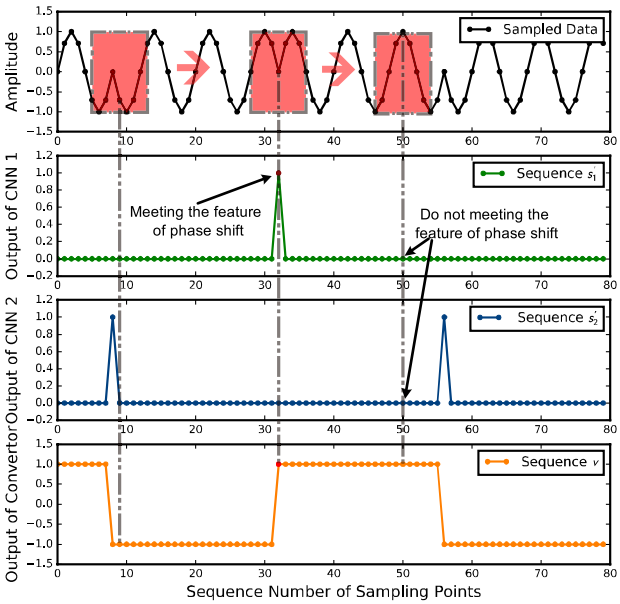

FIGURE 3. The corresponding relations of the inputs and the outputs of the neural network, and the outputs of convertor.

the neural network are approximately 0 and 1, two decision devices are utilized to judge the outputs and achieve the decision sequence of s'_1 and s'_2. Then, a convertor transforms the sequences of s'_1 and s'_2 into the sequence v, where the relations are shown in Fig. 3. Finally, the demodulated data can be achieved through the low pass filtering and timing sampling. Benefitting from the symbol synchronization module, the proposed demodulator can provide correct demodulation results even if the Doppler frequency offsets or the ADC sampling timer errors exist.

B. DETAILS OF THE 1-D CNN

1) TRAINING SET GENERATION

In order to improve the anti-noise capability of the proposed demodulator, the training sets are generated by the modulated data through AWGN channel in this paper. The number of samples in each carrier period is M. The discrete samples can be expressed as $x_r(n)$ $(n = 1, 2, 3, \ldots, N)$, where N is the total number of the samples, an integer multiplication of M. $x_r(n)$ can be represented as

$$x_r(n) = x_r(t_n) \tag{9}$$

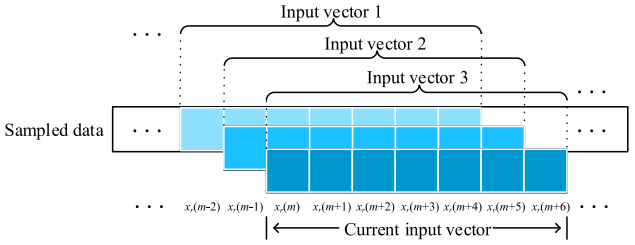

FIGURE 4. The relations between the input vector and the sequence of samples, compared with the last input vector, the current input vector has only one single point sliding.

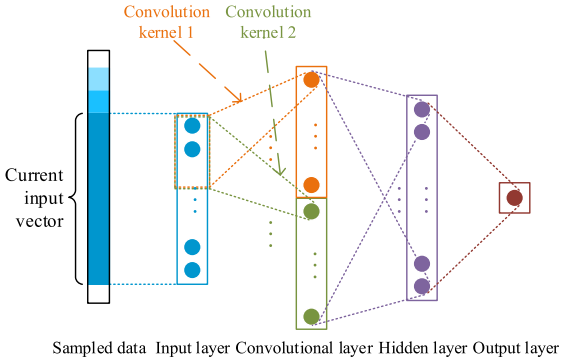

FIGURE 5. The architecture of the proposed 1-D CNN, which consists of an input layer, a convolutional layer, a hidden layer, and an output layer.

where t_n represents the sampling time corresponding to the nth samples.

$(M + 1)$ consecutive sampling points is taken from the sequence of samples as input vectors. Thus the input vector $\mathbf{x_m}$ can be expressed as

$$\mathbf{x_m} = \begin{bmatrix} x_r(m) \\ x_r(m+1) \\ x_r(m+2) \\ \vdots \\ x_r(m+M) \end{bmatrix}_{(M+1)\times 1} \qquad m = 1, 2, 3, \ldots, N - M \tag{10}$$

Fig. 4 illustrates the relationship between the input vector and the sequence of samples. The current input vector has only one single point sliding compared with the last input vector. In Fig. 3, an input vector is composed of the points covered by the red frame. With the red frame moving along the sampling sequence, the input data matrix is generated. This method avoids grouping the sampling sequence. Matching with the proposed 1-D CNN, the sampling points can be mapped to the points in the output sequence one by one.

The input data matrix is the aggregation of input vectors, which can be indicated as (11), as shown at the bottom of this page.

The dimension of the output vector is 1, and the output matrix is the aggregation of the output vectors, which is indicated as

$$Y_i = \begin{bmatrix} \mathbf{y_1^i} & \mathbf{y_2^i} & \mathbf{y_3^i} & \cdots & \mathbf{y_{N-M}^i} \end{bmatrix}_{1\times(N-M)} \qquad i = 1, 2 \tag{12}$$

where Y_1 denotes the expected output matrix of CNN 1, representing the phase shift from 0° to 180°, Y_2 is the expected output matrix of CNN 2, exhibits the phase shift from 180° to 0°. y_m^i takes either 0 or 1, indicating whether the input vector coincides with the features of the phase shifts. In the training process, sequence s_1 and s_2 are gradually approaching Y_1 and Y_2. In ideal cases we have $s_1' = Y_1$ and $s_2' = Y_2$, and the output of demodulator is absolutely correct.

2) ARCHITECTURE OF THE 1-D CNN

The proposed 1-D CNN demodulator is composed of two identical 1-D CNNs, and the architecture of 1-D CNN is depicted in Fig. 5.

The 1-D CNN consists of 4 layers, including an input layer, a convolutional layer, a hidden layer, and an output layer. The input layer has $(M + 1)$ nodes, which is identical to the length of the input vectors. The convolutional layer is applied to perform the neighborhood filtering [23] on the one-dimensional input signal. The two vectors separately exported by the two convolution kernels are merged into one vector and then imported to the hidden layer. The task of the hidden layer is to avoid the neural network from being trapped into local optimal solutions. An appropriate number of nodes is very important for the hidden layer. When there are fewer nodes in the hidden layer, the neural network is vulnerable to be trapped into the local optimum, and eventually the demodulator fails to work. On the other hand, when there are too many nodes in the hidden layer, the neural network hardly converges during the training. After performing sufficient tests, it is concluded that the best performance is achieved by setting the number of nodes as $(2M + 4)$. The output layer contains only one node, and its output is also the output of the

$$\begin{aligned} X &= \begin{bmatrix} \mathbf{x_1} & \mathbf{x_2} & \mathbf{x_3} & \cdots & \mathbf{x_{N-M}} \end{bmatrix}_{(M+1)\times(N-M)} \\ &= \begin{bmatrix} x_r(1) & x_r(2) & x_r(3) & \cdots & x_r(N-M) \\ x_r(2) & x_r(3) & x_r(4) & \cdots & x_r(N-M+1) \\ x_r(3) & x_r(4) & x_r(5) & \cdots & x_r(N-M+2) \\ \vdots & \vdots & \vdots & \ddots & \vdots \\ x_r(M+1) & x_r(M+2) & x_r(M+3) & \cdots & x_r(N) \end{bmatrix}_{(M+1)\times(N-M)} \end{aligned} \tag{11}$$

neural network, which represents whether the neural network has detected the phase shifts in the input vector.

The convolutional layer contains two convolution kernels, which have one-dimensional structure and possesses the same length as the input vector. The convolution kernel can be expressed as

$$\mathbf{k} = \begin{bmatrix} k_1 \\ k_2 \\ k_3 \\ \vdots \\ k_{M+1} \end{bmatrix}_{(M+1)\times 1} \tag{13}$$

The convolution kernel adopts the convolution style of same convolution, which means the output of the convolution has the same length with its input vector, and the output of the convolution kernel is given by

$$\mathbf{c} = \begin{bmatrix} c_1 \\ c_2 \\ c_3 \\ \vdots \\ c_{M+1} \end{bmatrix}_{(M+1)\times 1} = \mathrm{ReLU}(\mathbf{k} * \mathbf{x_m}) \tag{14}$$

where ReLU [24] indicates the activation function of the convolutional layer.

The convolutional layer is the core of the 1-D CNN demodulator, and it extracts the features of the phase shifts in the input vector. For a sequence processed by the convolutional layer, the points of the phase shift features will be highlighted, and the points of the non-phase shift features will be filtered.

Because of the existence of convolutional layer, the computational complexity of 1-D CNN is significantly lower than that of the MLP on a same scale. For the proposed 1-D CNN, it takes $(M+1)^2$ multiplications to obtain the convolutional layer's output. For MLP, it takes $2(M+1)^2$ multiplications to get the same size hidden layer output as convolutional layer's output of the proposed 1-D CNN. Therefore, compared with the neural network demodulator using MLP [15]–[18], the computational complexity of the proposed architecture is significantly reduced.

C. HANDLING STRATEGY FOR CARRIER FREQUENCY OFFSET

In the process of channel transmission, the carrier frequency offset and the sampling frequency error is inevitable. For conventional coherent demodulators, due to the existence of carrier synchronization, the demodulator is able to process some kind of frequency offsets. However, for a neural network demodulator, the frequency offset affects the input vector of the neural network.

Regarding to the carrier frequency offset, we assume the received signal as

$$x_r(t) = A\cos((\omega_c + \Delta\omega)t + \varphi_n) \tag{15}$$

where $\Delta\omega$ is the angular frequency offset of the received signals, and it is assumed as a constant. For a given received modulated signal, ADC is carried out at first, and the sampling times are $(t_1, t_2, t_3, \ldots, t_n)$. Assuming there is no error in sampling times, the nth sample is defined as

$$\begin{aligned} x_r(t_n) &= A\cos((\omega_c + \Delta\omega)t_n + \varphi_n) \\ &= A\cos(\omega_c t_n + (\Delta\omega t_n + \varphi_n)) \end{aligned} \tag{16}$$

According to (16), frequency offset is transformed into phase deviation at each specific sample. For a relatively large n, signals with frequency offset may present a large phase deviation. The scheme of the neural network demodulators proposed in [14]–[20] divide the samples with fixed numbers, each group is served as an input vector. Regarding to the $(k+1)$th input vector, each of samples has at least $\Delta\omega t(k\sigma+1)$ phase deviation. For a specified sampling period of T, when $\Delta\omega t(k\sigma+1) > \omega_c T$, the input vector of the neural network is not corresponded to the samples in a complete symbol period.

Regarding to the errors in the ADC sampling frequency, suppose a time difference between the expected sampling period and the authentic sampling period, as ΔT, and assuming that the initial sampling positions are the same. Hence, the nth sampling time can be expressed as

$$t_n' = t_n + (n-1)\Delta T \tag{17}$$

where t_n' is authentic sampling time, and t_n is expected sampling time. Then nth sample can be expressed as

$$\begin{aligned} x_r(t_n') &= A\cos(\omega_c(t_n + (n-1)\Delta T) + \varphi_n) \\ &= A\cos(\omega_c t_n + (n-1)\omega_c\Delta T + \varphi_n) \end{aligned} \tag{18}$$

Similarly, the phase error of each sample increases with the increase in the number of samples. When $(n-1)\Delta T > T$, it results in the failure of the correct correspondence from the input vectors to the samples in a complete symbol period.

For the proposed 1-D CNN, the input vector of the neural network is generated by using the procedure in Section III-B. For carrier frequency error $\Delta\omega$, the input vector, $\mathbf{x_m}$, as shown in (10), can be formulated as

$$\mathbf{x_m} = \begin{bmatrix} A\cos(\omega_c t_m + (\Delta\omega t_m + \varphi_m)) \\ A\cos(\omega_c t_{m+1} + (\Delta\omega t_{m+1} + \varphi_{m+1})) \\ A\cos(\omega_c t_{m+2} + (\Delta\omega t_{m+2} + \varphi_{m+2})) \\ \vdots \\ A\cos(\omega_c t_{m+M} + (\Delta\omega t_{m+M} + \varphi_{m+M})) \end{bmatrix}_{(M+1)\times 1} \tag{19}$$

The phase deviation of each element in the input vector constitute the vector $\Delta\boldsymbol{\varphi}$, which can be expressed as

$$\Delta\boldsymbol{\varphi} = \begin{bmatrix} \Delta\omega t_m \\ \Delta\omega t_{m+1} \\ \Delta\omega t_{m+2} \\ \vdots \\ \Delta\omega t_{m+M} \end{bmatrix}_{(M+1)\times 1} = \begin{bmatrix} \Delta\omega t_m \\ \Delta\omega(t_m + T) \\ \Delta\omega(t_m + 2T) \\ \vdots \\ \Delta\omega(t_m + MT) \end{bmatrix}_{(M+1)\times 1} \tag{20}$$

TABLE 1. Seventeen 1-D CNN demodulators are trained by seventeen sets of data separately, and another 1-D CNN demodulator is trained by all of these data sets. The performances of these demodulators are evaluated by validation sets with varied SNRs.

Training Set SNR	BER of Trained 1-D CNN Demodulators				
	Validation Set SNR=-2	Validation Set SNR=0	Validation Set SNR=2	Validation Set SNR=4	Validation Set SNR=6
-6	0.2493	0.1864	0.1269	0.0768	0.0363
-5	0.2232	0.1379	0.0654	0.0224	0.0045
-4	0.2256	0.1351	0.0588	0.0132	0.0013
-3	0.2245	0.1354	0.0548	0.0122	0.0014
-2	**0.2202**	**0.1334**	**0.0536**	**0.0111**	**0.0009**
-1	0.2315	0.1396	0.0583	0.0136	0.0010
0	0.2335	0.1397	0.0613	0.0140	0.0021
1	0.2363	0.1500	0.0685	0.0172	0.0023
2	0.2531	0.1645	0.0787	0.0205	0.0028
3	0.2558	0.1631	0.0761	0.0215	0.0029
4	0.2765	0.1916	0.0985	0.0332	0.0054
5	0.3220	0.2399	0.1416	0.0601	0.0130
6	0.3190	0.2407	0.1449	0.0605	0.0140
7	0.3347	0.2531	0.1538	0.0632	0.0152
8	0.3545	0.2808	0.1889	0.0923	0.0298
9	0.3527	0.2818	0.1874	0.1009	0.0354
10	0.3802	0.3152	0.2313	0.1330	0.0403
All (-6 to 10)	0.2370	0.1457	0.0618	0.0146	0.0017

For a relatively large m, since $\Delta\omega MT \ll \omega_c t_m$, $\Delta\omega\mu T$ ($\mu = 1, 2, \ldots, M$) can be neglected. Accordingly, each element in vector $\Delta\boldsymbol{\varphi}$ can be regarded as $\Delta\omega t_m$, and the same is true for the situation of ADC sampling frequency error. As a result, in each input vector, the carrier frequency error and the sampling frequency error are transformed into the phase error of samples. It will be confirmed in section IV-C that this phase error does not interfere in the proposed 1-D CNN detecting whether the features of the phase shifts occur in each input vector. Therefore, the 1-D CNN can still generate sequence s_1 and s_2 correctly. Although the errors introduced by the frequency offset and the sampling frequency errors is taken into sequence s_1 and s_2, thanks to the symbol synchronization, the timing errors can be calculated and calibrated. Hence, the proposed 1D-CNN demodulator has a well capacity for dealing with the errors caused by the carrier frequency offset.

IV. SIMULATION RESULTS

In this section, a series of simulations have been carried out to verify the BER performance of the proposed 1-D CNN demodulator. In the experiments, the carrier frequency F_c is 1 MHz, the sampling frequency F_s is 8 MHz, and the symbol rate equaling 1 Mbps is chosen to obtain the most points of phase shifts.

A sequence of 10000 random binary symbols is used as the baseband data, on which the modulation and sampling are performed with the aforementioned parameters. To enhance the generalization capability of the 1-D CNN, some white Gaussian noise is added to the modulated signals. The training set input matrix is generated according to (11), and the training set label matrix is generated referring to (12).

A. EFFECT OF THE TRAINING SET

The training sets are generated using the respective channel environments with different SNR ranging from −6 to 10 dB, providing 17 training sets. Accordingly, each training set yields one 1-D CNN demodulator, therefore seventeen 1-D CNN demodulators are produced. Another 1-D CNN demodulator is trained by all of these training sets. The training ends at 100 epochs, after which the training loss almost no longer declines. The acquired eighteen 1-D CNN demodulators are tested by validation sets to find the one that provides the best BER performance. In the experiment, five data sets with different SNR, −2 dB, 0 dB, 2dB, 4dB and 6 dB, are chosen as the validation sets. Table 1 and Fig. 6 shows the BER performance of the eighteen neural networks tested by different validation set.

Fig. 6 shows the relationship between the BER performance of the trained 1-D CNN demodulator and the SNR of the training set. As is shown in this figure, the variation of the training data SNR will lead to a different 1-D CNN demodulator performance. The 1-D CNN demodulator with SNR of training set equaling −2 dB provides the best BER performance, and this demodulator is called the optimal 1-D CNN demodulator. Table 1 also reflects that the 1-D CNN trained by all training sets does not have better performance than the optimal 1-D CNN demodulator.

After a 100-epoch training, the relationship between the SNR of training set and the loss of the neural network is

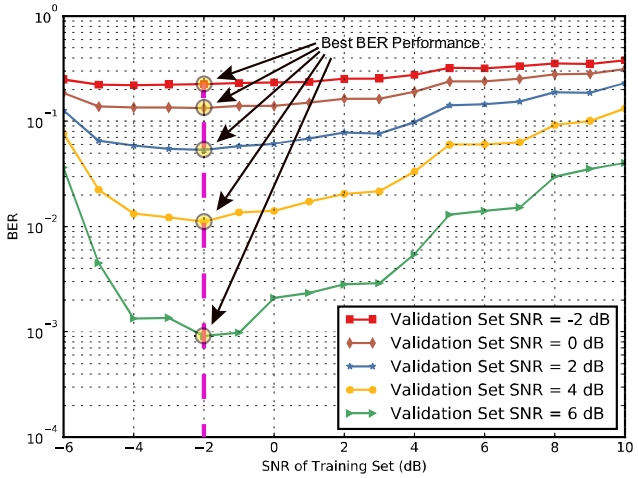

FIGURE 6. BER performance of the 1-D CNN demodulators trained by the data sets with different SNR ranging from −6 dB to 10 dB, the SNR of validation sets are −2dB, 0dB, 2dB, 4dB and 6dB.

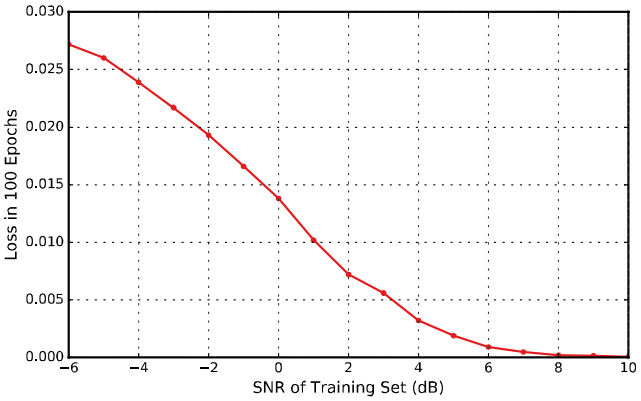

FIGURE 7. The relationship between training loss and SNR of training sets.

depicted in Fig. 7. From which we can see that the loss increases with the decrease of training set SNR. This is due to the fact that training set with lower SNR presents lower regularity, and consequently, results in lower speed of the neural network convergence. For the training sets with a relatively high SNR, it is easy for the neural network to learn how to extract the phase information from the training sets, and subsequently provides relatively lower training errors. However, at the same time, training sets with high SNR cause overfitting of the neural network. As a result, when dealing with the test sets with relatively higher noise, the neural network is unable to extract the phase information from them, which generates higher BER in demodulation. On the other hand, for the training sets with SNR lower than −2 dB, the BER of test sets increase rapidly. This is because the modulated waveforms is covered by the noise. At this time the training errors are comparatively higher, and the neural network is incapable of learning well on how to extract the phase information from the training sets.

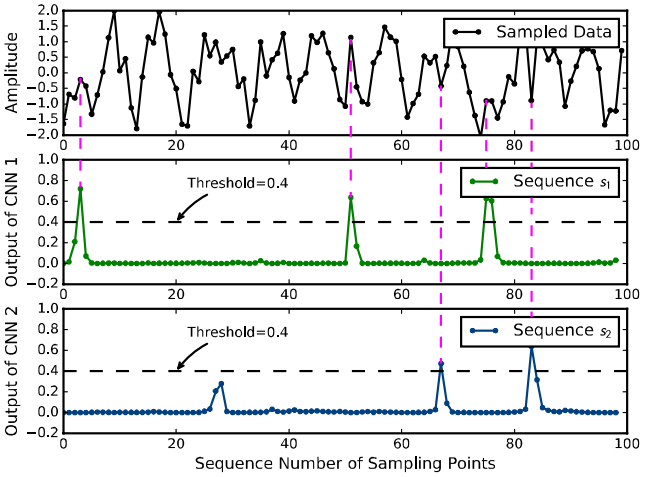

FIGURE 8. Inputs and outputs of the 1-D CNNs when the test data SNR equals 3dB.

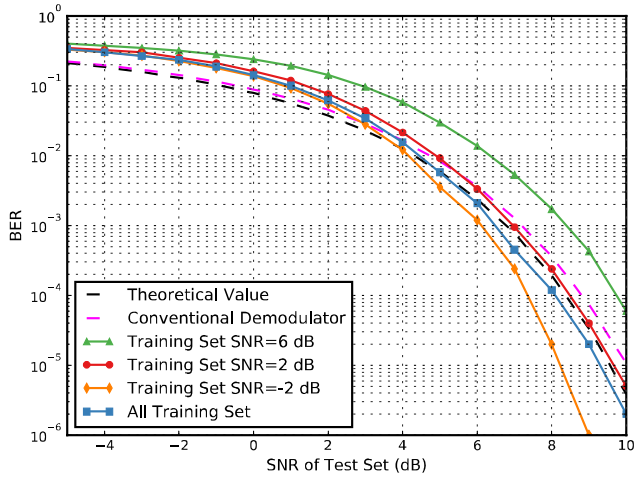

FIGURE 9. BER performance of the 1-D CNN demodulators with the training sets SNR equaling −2 dB, 2 dB, and 6 dB, and the other 1-D CNN demodulators is trained by all training sets. Theoretical values and simulation result of BER performance of conventional demodulator are also exhibited.

B. DEMODULATION PERFORMANCE IN DIFFERENT TEST SET

Fig. 8 presents the waveforms of the received modulated data with SNR equaling 3 dB, and the corresponding outputs of two 1-D CNNs. The output of neural network contains some certain errors, nonzero outputs appear when the input vector does not conform to the features of the phase shifts. As a result, a decision device is required after the outputs of the neural network to judge them. When the neural network output is greater than the given threshold, the decision device provides 1, otherwise it gives 0. The experimental results show that, the threshold equaling 0.4 provides the optimum value of the BER of the demodulation. The positions of phase shifts are marked with magenta lines. It can be seen that the outputs of CNN1 and CNN2 correctly indicate these phase shifts.

Fig. 9 shows the BER curve of a conventional demodulator and four 1-D CNN demodulators. As is shown in this figure, for the optimal 1-D CNN demodulator, its BER is lower than

the theoretical value when the SNR of the test sets are higher than 4 dB, presenting an about 0.4 dB gain compared with the theoretical value. Comparing the BER curves of the 1-D CNN demodulators with training sets SNR of -2 dB, 2 dB and 6 dB, the BER of the optimal 1-D CNN demodulator is always lower than them. For the 1-D CNN demodulator which trained by all training sets, its BER performance is between the 1-D CNN demodulator with the -2 dB training set and that with the 2dB training set. The BER curves of each 1-D CNN demodulator are not crossed, which reveals that the BER performance of 1-D CNN demodulator is stable.

From Fig. 9 we can see that the 1-D CNN demodulator trained by the -2 dB training set, which called the optimal 1-D CNN demodulator, has a better BER performance than the theoretical value. This is because the demodulation principle of the proposed 1-D CNN demodulator is different from that of the conventional method. The theoretical value of BPSK demodulation BER is calculated according to the misjudgment probability of the symbol. By contrast, the proposed 1-D CNN demodulator performs demodulation by directly judging the phase shifts. In the training phase, the neural networks learn some of the noise patterns and then take better decisions on phase shift judgment. Therefore, the performance of the 1-D CNN demodulator can exceed theoretical values.

C. DEMODULATION PERFORMANCE IN DIFFERENT SAMPLING PHASE DEVIATION

Assuming the ADC sampling period is T and without error, the phase deviation is identically the same at all samples in a test set, which is determined by the phase of initial sample point. For the sampled sequence with the initial sampling phase equaling 0, the sampling time of each points is 0, T, $2T$, $3T, \ldots, NT$. For the initial sampling phase of θ, the sampling time of each sample is $(\theta/2\pi)T$, $(1+\theta/2\pi)T$, $(2+\theta/2\pi)T, \ldots, (N+\theta/2\pi)T$. We generate ten test sets with the initial sample phase θ from 0 to 2π, and then test their BER with the optimal 1-D CNN demodulator. Fig. 10 (a) and Fig. 10 (b) depict the BER for the SNR of the test sets equaling 5 and 2 dB, respectively. The figures show that the initial sampling time has small influence on the BER. In other words, the proposed demodulator is not sensitive to the phase deviation of the sampling, which means no matter how much phase deviation it has, the 1-D CNN is capable of detecting the features of the phase shifts in the input vector. Experimental results prove that the proposed demodulator has the capabilities of dealing with carrier frequency offsets and the ADC sampling time errors, which has been analyzed in section III-C.

D. DEMODULATION PERFORMANCE IN FADING CHANNAL

During the transmission of modulated signal, the multipath effect may lead to Rayleigh fading. Inter symbol interference introduced by the multipath effect will affect the quality of signal transmission. Channel equalization is commonly used to eliminate inter symbol interference in Rayleigh fading. In this section, the performance of the proposed 1-D CNN in fading channel is tested.

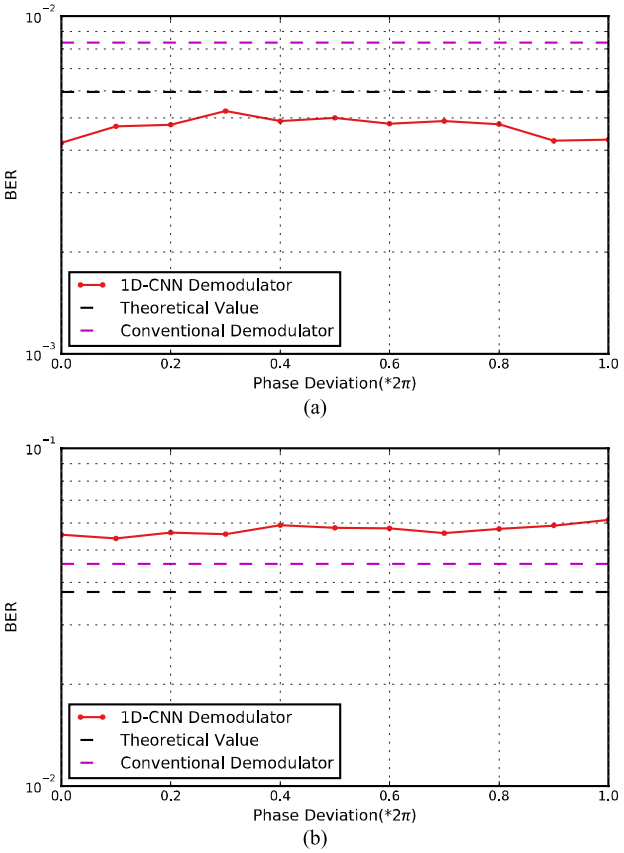

FIGURE 10. BER of the test sets for different sampling phases with (a) SNR of test sets equaling 5 dB, (b) SNR of test sets equaling 2 dB.

The training set is generated using the channel environment with Rayleigh fading, and then 1-D CNN is trained with it. The SNR of training set is set to -2 dB. For the trained 1-D CNN and the optimal 1-D CNN demodulator in section IV-A, the BER performance on Rayleigh fading channel is tested. The result is shown in Fig. 11, which indicates that the performance of the 1-D CNN demodulator trained by Rayleigh channel data is better than the optimal 1-D CNN demodulator. For the optimal 1-D CNN demodulator, it fails to deal with the impact of fading channel. But with the equalizer, the performance of the optimal 1-D CNN is close to the Rayleigh theoretical BER. Experimental results show that, training by fading channel data, the proposed 1-D CNN demodulator can eliminate the impact of Rayleigh fading.

E. COMPARISON WITH EXSITING METHODS

The comparison of the proposed 1-D CNN demodulator and other two neural network demodulator [17], [18] is shown in table 2. Both computational complexity and BER performance are compared. Under the condition of the modulation type is BPSK, the computational complexity of this paper

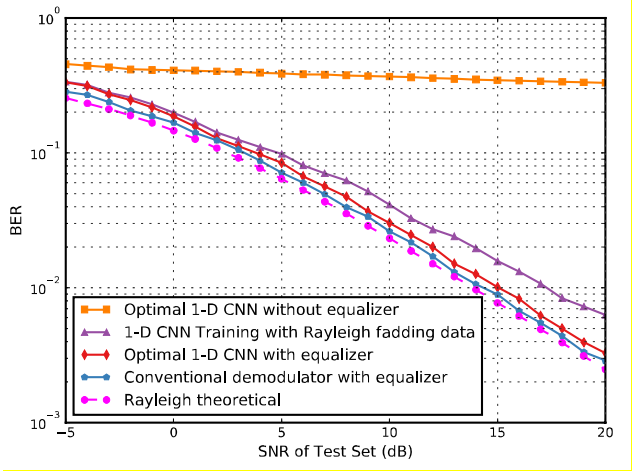

FIGURE 11. BER performance of the 1-D CNN in fading channel.

TABLE 2. Comparison of three neural network demodulators.

Neural Network		This Paper	MLP	MaxMLP
Modulation Type		BPSK	MPSK	Universal
Computational Complexity		$(M+1)^2$	$2(M+1)^2$	$2N(M+1)^2$
BER	SNR=0dB	0.1334	0.0792	0.0894
	SNR=4dB	0.0111	0.0127	0.0126
	SNR=6dB	0.0009	0.0025	0.0026

is $(M+1)^2$, while those of [17] and [18] are $2(M+1)^2$ and $2N(M+1)^2$, respectively. As for the BER performance, the proposed demodulator has better achievements in high SNR conditions. In addition, [17] and [18] both map the input of neural network into symbol directly, which is easily influenced by the carrier frequency offset and the sampling frequency error. For the 1-D CNN demodulator, the demodulation function is realized by detecting phase shifts, and that avoids the problems of grouping sampling sequences.

V. CONCLUSION

This paper proposes a 1-D CNN based BPSK demodulator, which is composed of two 4-layer CNNs, two decision devices, a convertor, and a symbol synchronization module. It utilizes two CNNs to detect two types of phase shifts, and extract the information from the phase message. The symbol synchronization is applied to deal with the errors caused by the carrier frequency offsets. Experimental results indicate that the proposed 1-D CNN can accurately detect the phase shifts of the BPSK modulated signals, even if some carrier frequency offsets and ADC sampling time errors exist. Employing the modulated signals with white Gaussian noise and Rayleigh fading as the training set enables the neural network to deal with AWGN and fading channel interference. It is when the training set SNR equals -2 dB that the 1-D CNN demodulator with the optimal demodulation performance achieves, in which case the BER performance of the demodulator in AWGN channel is close to the theoretical BER. When the SNR of the test set is greater than 4 dB, it provides 0.4 dB gain in comparison with its theoretical value.

REFERENCES

[1] C. Xu, X. Liu, and X. Wei, "Differential phase-shift keying for high spectral efficiency optical transmissions," *IEEE J. Sel. Topics Quantum Electron.*, vol. 10, no. 2, pp. 281–293, Mar. 2004.

[2] Y. Hu and M. Sawan, "A fully integrated low-power BPSK demodulator for implantable medical devices," *IEEE Trans. Circuits Syst. I, Reg. Papers*, vol. 52, no. 12, pp. 2552–2562, Dec. 2005.

[3] Z. Luo and S. Sonkusale, "A novel BPSK demodulator for biological implants," *IEEE Trans. Circuits Syst. I, Reg. Papers*, vol. 55, no. 6, pp. 1478–1484, Jul. 2008.

[4] W. Xu, Z. Luo, and S. Sonkusale, "Fully digital BPSK demodulator and multilevel LSK back telemetry for biomedical implant transceivers," *IEEE Trans. Circuits Syst. II, Exp. Briefs*, vol. 56, no. 9, pp. 714–718, Sep. 2009.

[5] G. A. Leonov, N. V. Kuznetsov, M. V. Yuldashev, and R. V. Yuldashev, "Nonlinear dynamical model of Costas loop and an approach to the analysis of its stability in the large," *Signal Process.*, vol. 108, pp. 124–135, Mar. 2015.

[6] Y. Bengio, I. J. Goodfellow, and A. Courville. (2016). *Deep Learning*. [Online]. Available: http://www.deeplearningbook.org

[7] M. N. Seyman and N. Taşpinar, "Channel estimation based on neural network in space time block coded MIMO–OFDM system," *Digital Signal Process.*, vol. 23, pp. 275–280, Jan. 2013.

[8] M. L. D. Wong and A. K. Nandi, "Automatic digital modulation recognition using artificial neural network and genetic algorithm," *Signal Process.*, vol. 84, no. 2, pp. 351–365, 2004.

[9] A. K. Nandi and E. E. Azzouz, "Modulation recognition using artificial neural networks," *Signal Process.*, vol. 56, no. 2, pp. 165–175, 1997.

[10] A. K. Pradhan, S. K. Meher, and A. Routray, "Communication channel equalization using wavelet network," *Digital Signal Process.*, vol. 16, pp. 445–452, Jul. 2006.

[11] Q. Xiao, G. Ge, and J. Wang, "The neural network adaptive filter model based on wavelet transform," in *Proc. 9th Int. Conf. Hybrid Intell. Syst.*, 2009, pp. 529–534.

[12] X. Cui, T. A. Gulliver, H. Song, and J. Li, "Real-time positioning based on millimeter wave device to device communications," *IEEE Access*, vol. 4, pp. 5520–5530, 2016.

[13] A. Patnaik, D. E. Anagnostou, R. K. Mishra, ChristodoulouCG, and J. C. Lyke, "Applications of neural networks in wireless communications," *IEEE Antennas Propag. Mag.*, vol. 46, no. 3, pp. 130–137, Jun. 2004.

[14] K. Nakayama and K. Imai, "A neural demodulator for amplitude shift keying signals," in *Proc. IEEE World Congr. Comput. Intell.*, Jun./Jul. 1994, pp. 3909–3914.

[15] S. Choi and D. Hong, "A hybrid structured neural network receiver in digital communication systems," in *Proc. IEEE-INNS-ENNS Int. Joint Conf. Neural Netw.*, Jul. 2000, pp. 378–383.

[16] M. R. Amini and E. Balarastaghi, "Improving ANN BFSK demodulator performance with training data sequence sent by transmitter," in *Proc. 2nd Int. Conf. Mach. Learn. Comput.*, 2010, pp. 276–281.

[17] F. He, X. Xu, L. Zhou, and H. Man, "A learning based cognitive radio receiver," in *Proc. Military Commubications Conf.*, 2011, pp. 7–12.

[18] M. Önder, A. Akan, and H. Doğan, "Advanced neural network receiver design to combat multiple channel impairments," *Turkish J. Electr. Eng. Comput. Sci.*, vol. 24, pp. 3066–3077, Apr. 2016.

[19] A. Aiello, D. Grimaldi, and S. Rapuano, "GMSK neural network based demodulator," in *Proc. Int. Data Acquisition Adv. Comput. Syst., Technol. Appl.*, 2001, pp. 2–6.

[20] M. Li, H. Zhong, and M. Li, "Neural network demodulator for frequency shift keying," in *Proc. Int. Conf. Comput. Sci. Softw. Eng.*, 2008, pp. 843–846.

[21] M. Fan and L. Wu, "Demodulator based on deep belief networks in communication system," in *Proc. Int. Conf. Commun., Control, Comput. Electron. Eng.*, 2017, pp. 1–5.

[22] D. Elbaz and M. Zibulevsky. (Oct. 2017). "End to end deep neural network frequency demodulation of speech signals." [Online]. Available: https://arxiv.org/abs/1704.02046
[23] S. Karuppanagounder and P. Shanmugavadivu, "Impulsive noise detection by second-order differential image and noise removal using adaptive nearest neighbourhood filter," *AEUE-Int. J. Electron. Commun.*, vol. 62, no. 6, pp. 472–477, 2008.
[24] A. L. Maas, A. Y. Hannun, and A. Y. Ng, "Rectifier nonlinearities improve neural network acoustic models," in *Proc. Int. Conf. Mach. Learn.*, 2013, vol. 30. no. 1, p. 3.

MIN ZHANG received the B.E. and M.E. degrees in measurement and control from Xidian University, where she is currently pursuing the Ph.D. degree in measurement and instrument. Her research interests are time and frequency measurements and digital signal processing.

ZONGYAN LIU received the B.E. degree in measurement and control technology and instrument from Xidian University, Xi'an, China, in 2015, where he is currently pursuing the M.E. degree. His current research interests are digital communication and pattern recognition.

LI LI received the B.E. and M.E. degrees in communication engineering from Xidian University in 1998 and 2008, respectively. He is currently a Research Engineer with CAST, China. His current research interests are communication signal modulation and data transmission systems.

HAI WANG received the B.E. degree in communication engineering, the M.E. degree in communication and information system, and the Ph.D. degree in measurement and instrument from Xidian University, Xi'an, China. He is currently an Associate Professor with Xidian University. His main research interests are the time and frequency measurements. His current research activities are focused on the frequency and phase measurements methods based on field-programmable gate array and system-on-a-programmable-chip, electronic instrument design, and time–frequency signal processing.